

# Electron-beam-induced current and cathodoluminescence characterization of InGaAs strain-balanced multiquantum well photovoltaic cells

Stefania Tundo

*Dipartimenti Ingegneria dell'Innovazione, Università di Lecce, via Monteroni, 73100, Lecce, Italy*

Massimo Mazzer<sup>a)</sup>

*CNR-IMM, Sezione di Lecce, Univ. Campus, via Arnesano, 73100 Lecce, Italy and Experimental Solid State Physics, Imperial College London, London, SW7 2AZ, United Kingdom*

Lucia Nasi, Laura Lazzarini, and Giancarlo Salviati

*CNR-IMEM Sezione di Parma, Parco Area delle Scienze 37/A, 43010 Fontanini-PR, Italy*

Carsten Rohr, Paul Abbott, David B. Bushnell, and Keith W. J. Barnham

*Experimental Solid State Physics, Imperial College London, London, SW7 2AZ, United Kingdom*

Graham Clarke

*IQE Limited, Cardiff, Wales, United Kingdom*

Ruwen Peng

*National Laboratory of Solid State Microstructures, Nanjing University, Nanjing 210093, China*

(Received 22 July 2003; accepted 26 August 2003)

$\text{In}_x\text{Ga}_{1-x}\text{As}/\text{In}_y\text{Ga}_{1-y}\text{As}$  strain-balanced quantum well cells (QWCs) have been shown to be beneficial for photovoltaic applications in particular to extend the light absorption edge of a single-junction cell toward the near infrared with a lower reduction of the open-circuit voltage compared to a single band-gap cell. The strain-balancing condition ensures that the multi-quantum well as a whole does not relax. However, if the mismatch between wells and barriers exceeds a critical limit, the structure becomes vulnerable to morphological or compositional fluctuations, which can lead to a local structural breakdown with the generation of extended defects of a completely different nature from misfit dislocations. In this work, we investigated a series of strain-balanced InGaAs QWCs grown on InP for thermophotovoltaic applications by means of electron-beam-induced current (EBIC) and cathodoluminescence (CL) measurements. Despite being electrically active, these defects appear to have a minor impact on the dark current of the cells but cause a drop of the photocurrent at relatively low forward bias voltage. The higher carrier collection efficiency revealed both by EBIC and CL at the boundaries of the defects suggests that a notch in the valence band edge limits the collection of holes generated in the MQW and the energy states, induced by the defects inside the energy gap, assist the tunneling of holes through the notch. At zero bias, the overall reduction of the collection efficiency is of the order of a few percent but the rate of recombination of photogenerated carriers increases dramatically with increasing forward-bias voltage as the junction built-in field drops more rapidly where the density of in-gap states is higher.

© 2003 American Institute of Physics. [DOI: 10.1063/1.1618924]

## I. INTRODUCTION

Quantum well photovoltaic cells (QWCs), proposed and developed at Imperial College London<sup>1</sup> are now a well established technology in what is called “third-generation photovoltaics”<sup>2</sup> and in particular for solar concentrators<sup>3</sup> and thermophotovoltaic applications.<sup>4</sup> Among the advantages of QWCs, the insertion of multiquantum wells (MQWs) in the intrinsic region of a *p-i-n* junction makes it possible to tune the spectral quantum efficiency of the cells by changing the thickness and the composition of the wells. However, in most of the cases, this degree of freedom is limited by the conditions for the structural stability of epitaxially grown MQWs particularly in the case of the most interesting material for this technology, that is InGaAs (Ref. 5) whose lattice

parameter varies by as much as 7% between the two limiting binary compounds, GaAs and InAs. The concept of strain-balanced (SB)-QWC has proven to be the most effective solution to ensure the growth of several tens of periods of highly mismatched wells and barriers<sup>6–8</sup> without the generation of misfit dislocations which have been proven to be highly detrimental in the case, for instance, of InGaAs/GaAs MQWs grown on GaAs substrates.<sup>9,10</sup>

In a SB-QWC, the composition of the layers is chosen in such a way that the total elastic force exerted by the compressively stressed wells is balanced by the overall tensile force due to the barriers.<sup>11</sup> The absorption edge of an InGaAs SB-QWC can be moved toward higher wavelengths by increasing the indium content in the wells which, in turn, requires the increase of either the gallium content or the thickness of the barriers to preserve the balance of the overall

<sup>a)</sup>Electronic mail: m.mazzer@imperial.ac.uk

structure. However, although the balancing condition ensures that the MQW as a whole does not relax, there is a limit in the mismatch between wells and barriers beyond which any small structural irregularity in the MQW, such as the onset of a wavy morphology, is rapidly amplified by the large strain fields in the multilayer stack and may eventually lead to the local collapse of the structure.<sup>12</sup>

In this article, we analyze the electro-optical properties of the defects originating from the structural breakdown of SB  $\text{In}_x\text{Ga}_{1-x}\text{As}/\text{In}_y\text{Ga}_{1-y}\text{As}$  MQWs grown on InP and their impact on the performance of a QWC for thermophotovoltaic applications. Whereas, in the case of a strained MQW, misfit dislocations cause a dramatic increase of the (forward bias) dark current even at a relatively low density,<sup>9</sup> we show that the extended defects resulting from the collapse of a SB-QWC, called SB defects, have a comparatively negligible effect on the dark current of the cell. At the same time, however, they have a major impact on the photocurrent, that is, on the collection efficiency of the junction which causes a strong degradation of both the fill factor and the open-circuit voltage with respect to a reference sample with no quantum wells under the same blackbody illumination.

Electron-beam-induced current (EBIC) and cathodoluminescence (CL) were used to study the nature of the SB defects and to explain the links with the electrical properties of the cells. The results show that both the CL (open circuit) and the EBIC (short circuit) contrast are determined by the interplay between the nonradiative recombination strength of the SB defects and the electric dipole field at the interface between the InGaAs MQW and the wider band-gap (InGaAsP) emitter.

## II. EXPERIMENT

The samples investigated in this work are based on 30 period  $\text{In}_y\text{Ga}_{1-y}\text{As}/\text{In}_x\text{Ga}_{1-x}\text{As}$  SB MQWs, incorporated in the intrinsic region of an InP *p-i-n* junction grown by metal organic vapor phase epitaxy on (100) InP substrates. An unintentionally doped InP or InGaAsP buffer layer is deposited between the MQW and the InP *p* layer to prevent zinc diffusion into the intrinsic region. Compositions and thickness of wells and barriers were designed in order to obtain an absorption edge between 1700 and 2000 nm. The details of these samples are reported in Ref. 13 together with the transmission electron microscopy (TEM) and x-ray diffraction (XRD) results.

The electrical characteristics of the devices were measured both in the dark and under illumination. The equipment consisted of a Keithley 238 source measure unit and a Keithley 142 DIGITAL multimeter connected to a platinum resistance thermometer.

The TEM analysis was performed on a JEOL 2000FX microscope operated at 200 kV. Observations were made on (100) plan-view and  $(-110)$  cross section specimens with diffraction vectors  $g=(2\ 2\ 0)$  and  $g=(2\ 0\ 0)$  which are known to be highly sensitive to strain field and chemical composition, respectively.

The EBIC observations were performed in a Philips XL20 scanning electron microscope equipped with a variable

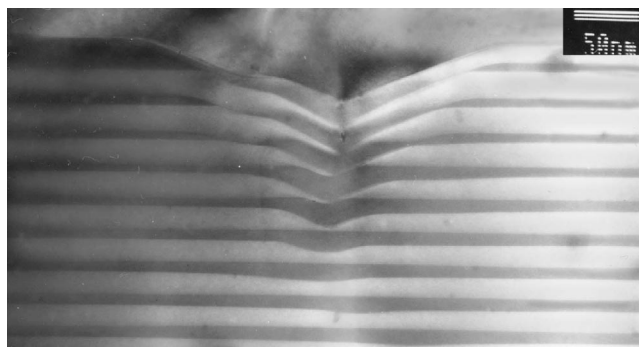


FIG. 1. Bright-field ( $g=002$ ) TEM image showing a defect cluster in cross section. Wells and barriers correspond to darker and brighter layers, respectively.

gain current amplifier (Keithley 428). The samples were observed in plan view (*p*-balanced layer on top) at room temperature. The induced current was collected through two gold electric contacts to the *p* and *n* regions. Finally, the CL investigations were performed at 80 K, on a Cambridge Stereoscan 350 scanning electron microscope (SEM) equipped with a Gatan mono-CL system.

## III. RESULTS AND DISCUSSION

### A. Formation of strain-balanced defects

The TEM and XRD analysis presented in Ref. 12 showed that the maximum number of defect free periods in a InGaAs SB MQW is proportional to the inverse of the elastic energy density per unit area stored in each period. The route to the structural breakdown is triggered by the onset of a surface undulation leading to a thickness modulation in the MQW.

The MQW thickness modulations always start in the tensile barrier layers and propagate vertically with increasing amplitude through the MQW structure (see Fig. 1). It is also observed that wells and barriers are modulated in opposite phase and eventually columns of highly stressed material are developed. These highly stressed regions are the favorite sites for the local occurrence of a catastrophic plastic relaxation whose probability increases with increasing lattice mismatch between wells and barriers. The local collapse of one of either the tensile-strained or compressively strained layers breaks the balance in favor of the lattice parameter of one of the two materials. As a result, the threshold for the onset of a three-dimensional growth regime can be exceeded for the complementary layer and a cluster of extended defects develops rapidly.

The SB defect clusters do not interact with each other and consist of stacking faults and dislocations originating in the MQW and threading up to the free surface of the heterostructure. Moreover, the defected regions are generally associated with a growth rate reduction which leads to the development of deep depressions on the free surface.<sup>13</sup> These morphological features are also clearly visible in the secondary-electron images of the surface obtained by the SEM and are always correlated with both the EBIC and the

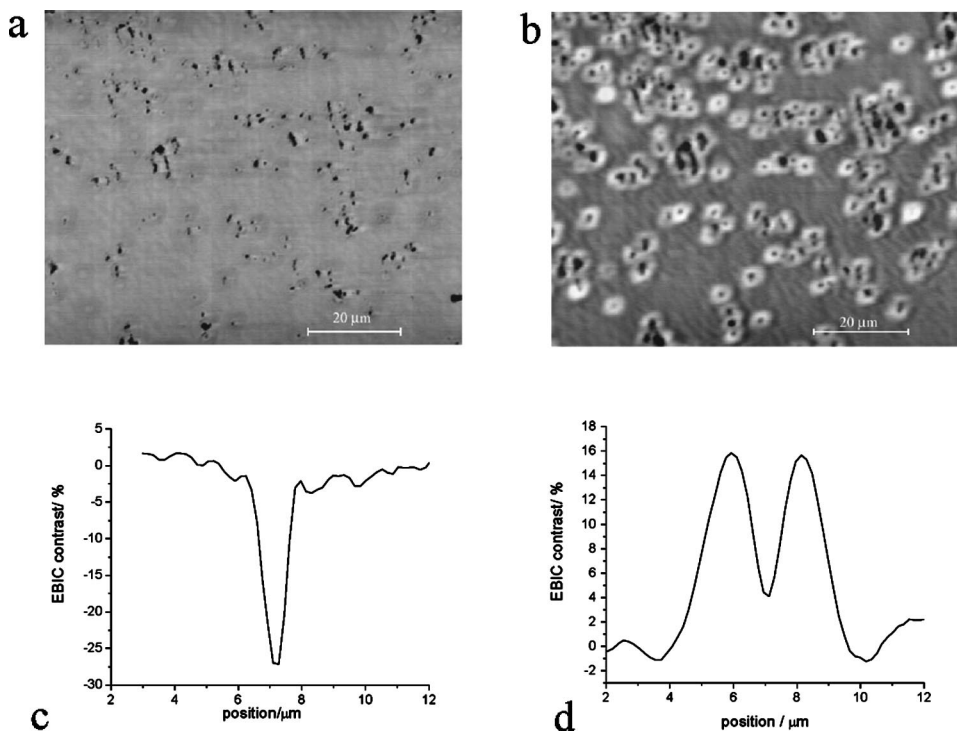


FIG. 2. EBIC maps showing the contrast generated by the SB defects at a beam voltage of 5 kV (a) and of 20 kV (b). The current profiles across one of the SB defects at 5 kV (c) and at 20 kV (d).

CL contrast patterns (in the case of CL see Fig. 3) presented and discussed in the next two paragraphs.

### B. Electron-beam-induced current results

The EBIC images at several values of the electron-beam accelerating voltage, reveal that besides the contrast produced by the SB defects no plastic relaxation occurred at the interface between the SB MQW and  $n$  region, that is the overall stress balancing is not affected by the local lattice breakdown and no misfit dislocations are observed. This is true for all the samples above the stability threshold, SB defects, and misfit dislocations appearing to be mutually exclusive.

The EBIC micrograph at 5 keV [Fig. 2(a)] shows a distribution of dark spots suggesting the obvious conclusion that the SB defects are sites of strong nonradiative recombination centers mainly associated with the dangling bonds at the dislocation cores. The same pattern is obtained up to just above 10 keV, that is for an electron beam generating most of the electron-hole pairs inside the  $p$  region of the junction.

However, a further increase of the accelerating voltage brings about a rapid change of the contrast pattern with the appearance of increasingly stronger bright halos around most of the dark spots. At 20 keV [Fig. 2(b)], when the generation volume includes the whole of the intrinsic region and reaches the  $n$  region, the relative increase of the EBIC signal (positive contrast) at the border of the defects with respect to background signal away from the defects is comparable to and in many cases exceeds the relative reduction (negative contrast) due to the nonradiative recombination [see Figs. 2(c) and 2(d)].

### C. Cathodoluminescence results

At a first glance, CL seems to give quite a different result, the panchromatic image at 20 keV shows just a collection of dark spots with no sign of bright halos [Fig. 3(a)]. These images are more similar to the EBIC micrographs at 5 keV, although they are less defined due to the higher beam acceleration voltage.

The absence of any bright contrast in the panchromatic CL images rules out the possibility that the contrast inversion in the EBIC images at high acceleration voltage is due to a larger gain, that is, to a greater number of electron-hole pairs generated per incident electron at the boundaries of the SB defects with respect to the defect-free areas. Therefore, the bright halos in EBIC must be caused by a greater carrier collection efficiency although, at that accelerating voltage, the overwhelming majority of carriers are generated in the depletion region in the presence of a strong electric field. In other words, the collection of photogenerated carriers appears to be reduced by an energy barrier at the interface between the low and the high band-gap material apart from a small region near the defect boundaries.

The confirmation is provided by the monochromatic CL images collected at different wavelengths. The most important result is the map at 1080 nm, that is, at the peak of the emission by the quaternary layer ( $p$  region at the border with the intrinsic region), where the dot-halo type contrast is again observed like in the EBIC maps collected at 20 kV [Fig. 3(b)]. However, the image at the peak of the MQW emission [Fig. 3(c)], shows a pattern similar to the panchromatic map but with wider black spots.

This behavior is consistent with the hypothesis described above. In fact, the bright contrast at 1080 nm is generated by the extra carriers which overcome the potential barrier at the

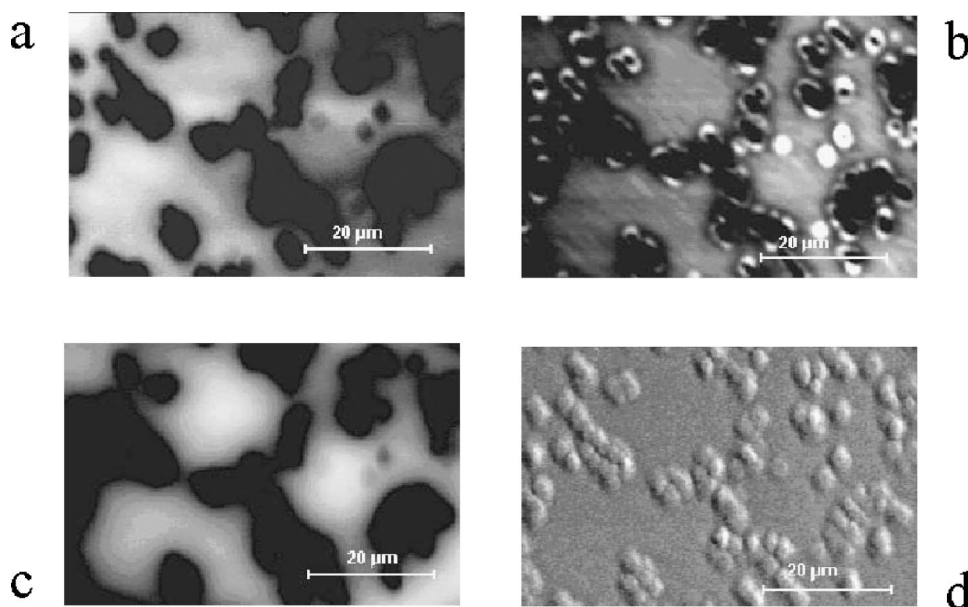


FIG. 3. CL maps at 80 K and with a beam acceleration voltage of 20 kV: Panchromatic map (a), monochromatic map at 1080 nm corresponding to the peak emission from the InGaAsP buffer layer (b), and monochromatic map at 1645 nm corresponding to the peak emission of the MQW (c). The topographic secondary-electron image of the same area of the sample is also shown (d).

heterointerface between the intrinsic and the  $p$  region and recombine radiatively in the InGaAsP layer. At the same time, the additional photocarriers collected by the junction are subtracted from those which generate the luminescence signal from the intrinsic region. This is the reason why the halos, which are bright at 1080 nm, turn dark at the MQW peak.

Finally, the panchromatic CL map is determined by the overall balance between radiative and nonradiative recombination in the sample. Therefore, being nonradiative recombination centers, the SB defects produce a dark contrast as expected.

#### D. Explanation of the electron-beam-induced current and the cathodoluminescence contrast

The key to explaining the EBIC and CL results is the heterointerface between the InGaAs MQW and the unintentionally doped InGaAsP (or InP) buffer layer which is doped by zinc diffusing from a  $2 \times 10^{18}$  doped layer of InP grown at the top. This solution is used to avoid the penetration of Zn into the intrinsic region of the photovoltaic cell where it would cause a major deterioration of the carrier collection efficiency. However, if the zinc diffusion into the buffer layer is insufficient, the band alignment at the heterointerface with the lower band-gap MQW gives rise to a notch in the valence-band edge with a formation of a hole accumulation layer at the lower band-gap side of the interface. Figure 4(a) is a sketch of the interface between the buffer layer and the MQW showing the notch which inhibits the collection of holes photogenerated in the MQW.

At short circuit, that is, under the EBIC experimental conditions, the large built-in field outbalances the effect of this barrier, the reduction of the collection efficiency being at most of the order of a few percent. However, at the boundaries of the SB defects, the high density of in-gap electron states associated with the extended defects, assists the tunneling of holes through the barrier and is responsible for the bright halos observed in the EBIC maps at 20 kV when most

of the electron-hole pairs are generated in the MQW. The CL maps at 20 kV confirm that the tunneling of photogenerated holes is effective also under open-circuit conditions, that is under low forward-bias conditions.

#### E. Correlation with the cell electrical properties

As the forward-bias voltage increases the built-in field decreases more rapidly in the highly defected region where

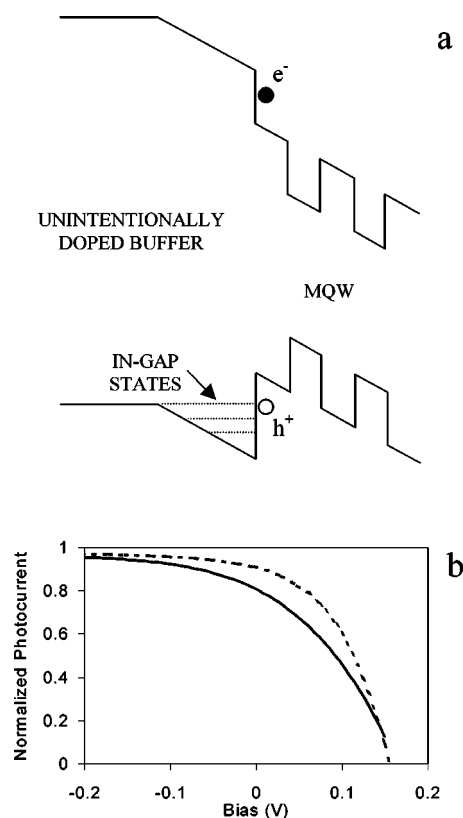


FIG. 4. Schematic band diagram of the  $p$ - $i$  interface of the junction (a). Monochromatic  $I$ - $V$  curves of a defected cell at 25 °C at 800 nm (broken line) and 1800 nm (solid line).

the bare charge at the defect boundaries tends to be compensated by the free charges. At the same time and for the same reason, the lateral field generated by the charged boundaries drops and the probability for a photogenerated carrier to be captured by a nonradiative recombination center in the low band-gap material increases. As a result, the collection efficiency for the charges generated in the MQW is expected to drop dramatically.

In fact, the light current–voltage ( $I$ – $V$ ) response of the MQW cell under a 3000 K blackbody source shows that the photocurrent falls off faster with increasing forward bias compared to a similar sample with the absorption edge at a lower wavelength and no SB defects. A measure of the poor performance of the cell is given by the fill factor which is lower than 50%. At the same time, however, the dark current of the two samples is comparable despite the presence of the nonradiative recombination centers. The main reason is that the SB defects originate in the MQW and most of the nonradiative recombination centers are distributed either in the  $p$  region or near the  $p$ – $i$  interface where the electron density is very low due to the heterojunction field.

A further confirmation of this interpretation is given by the  $I$ – $V$  curves under monochromatic illumination which show that the reduction of the collection efficiency with increasing forward-bias voltage is more important the longer the wavelength of the incident radiation [see Fig. 4(b)]. In fact, photons with energies greater (i.e., smaller wavelengths) than the InGaAsP band gap are absorbed mainly in the emitter ( $p$  region), where the minority carriers are electrons which do not experience any barrier at the  $p$ – $i$  interface. Photons with lower energy can only be absorbed (if above the effective band-gap energy) by the MQW where holes contribute to the photocurrent and, therefore, the effect of the interface barrier becomes significant. For this reason, the  $I$ – $V$  response improves by decreasing the light wavelength.

#### IV. CONCLUSIONS

The presence of anomalous bright boundaries in the EBIC and CL maps of a series of SB MQW photovoltaic

cells were explained in terms of the interplay between the structural properties of the extended defects arising from the local breakdown of the structure and the electrical properties of the  $p$ – $i$ – $n$  junction. In particular, the poor fill factor of the cells was found to be triggered by the valence-band notch at the heterointerface between the low band-gap  $i$  region and the emitter which enhances the rate by which photogenerated holes are trapped by the nonradiative recombination centers even at very low forward-bias conditions.

#### ACKNOWLEDGMENT

This work has been partially supported by the EC Grant Nos. ERK6-CT-1999-00019 and ICB1-CT-2000-80.012.

- <sup>1</sup>K. Barnham *et al.*, Proceedings of the Third World Conference of Photovoltaic Energy Conversion (WCPEC-3), Osaka, (2003).
- <sup>2</sup>M. A. Green, *Electrochem. Soc. Proc.* **10**, 30 (2001).
- <sup>3</sup>T. N. Tibbits *et al.* Proceedings of the Third World Conference of Photovoltaic Energy Conversion (WCPEC-3), Osaka, (2003).
- <sup>4</sup>C. Rohr, J. P. Connolly, N. Ekins-Daukes, P. Abbott, I. Ballard, K. W. J. Barnham, M. Mazzer, and C. Button, *Physica E (Amsterdam)* **14**, 158 (2002).
- <sup>5</sup>A. Zachariou *et al.*, Proceedings of the Second World Conference of Photovoltaic PV Solar Energy Conversion, (1998), p. 223.
- <sup>6</sup>N. Ekins-Daukes, K. W. J. Barnham, J. Connolly, J. Roberts, J. C. Clark, G. Hill, and M. Mazzer, *Appl. Phys. Lett.* **75**, 4195 (1999).
- <sup>7</sup>D. B. Bushnell *et al.*, Proceedings of the Third World Conference of Photovoltaic Energy Conversion (WCPEC-3), Osaka, (2003).
- <sup>8</sup>P. Abbott, C. Rohr, J. P. Connolly, I. Ballard, K. W. J. Barnham, R. Ginige, G. Clarke, L. Nasi, and M. Mazzer, *AIP Conf. Proc.* **653**, 213 (2003).
- <sup>9</sup>P. R. Griffin, J. Barnes, K. W. J. Barnham, G. Haarpaintner, M. Mazzer, C. Zanotti-Fregonara, E. Grunbaum, C. Olson, C. Rohr, J. P. R. David, J. S. Roberts, R. Grey, and M. A. Pate, *J. Appl. Phys.* **80**, 5815 (1996).
- <sup>10</sup>M. Mazzer, E. Grunbaum, K. W. J. Barnham, J. Barnes, P. R. Griffin, D. B. Holt, J. L. Hutchison, A. G. Norman, J. P. R. David, J. S. Roberts, and R. Grey, *Mater. Sci. Eng., B* **42**, 43 (1996).
- <sup>11</sup>N. J. Ekins-Daukes, J. M. Barnes, K. W. J. Barnham, J. P. Connolly, M. Mazzer, J. C. Clark, R. Grey, G. Hill, M. A. Pate, and J. S. Roberts, *Sol. Energy Mater. Sol. Cells* **68**, 71 (2001).
- <sup>12</sup>L. Nasi, C. Ferrari, L. Lazzarini, and G. Clarke, *J. Appl. Phys.* **92**, 7678 (2002).
- <sup>13</sup>L. Nasi, C. Ferrari, L. Lazzarini, G. Salviati, S. Tundo, M. Mazzer, G. Clarke, and C. Rohr, *J. Phys.: Condens. Matter* **14**, 13367 (2002).